Effects of Contact Angle on the Dynamics of Water Droplet Impingement

Junling Hu[*1], Xingguo Xiong[2] , Huang Xiao[3], Kai-tak Wan[3]
[1]Department of Mechanical Engineering, University of Bridgeport, Bridgeport, CT 06604 USA
[2]Department of Electrical and Computer Engineering, University of Bridgeport, Bridgeport, CT 06604 USA
[3]Department of Mechanical and Industrial Engineering, Northeastern University, Boston, MA 02115 USA
*jjhu@bridgeport.edu

Abstract: This paper simulated the dynamic process of a water droplet impinging onto a wax substrate in COMSOL, using the Phase Field method for tracking the free surface. The predicted spreading factor and apex height agree well with the experimental results during the initial dynamic impingement process, but the discrepancy between the simulation and experimental results increases in the later spreading and receding stages. Three contact angle models were implemented and the simulation results were compared to study the effects of the contact angle on the impingement process. It was found that a dynamic contact angle model is important for accurately modeling the droplet spreading and receding process. The instantaneous evolution of the dynamic contact angle cannot be represented by a constant static contact angle or the advancing-receding static contact angles. The simulation results can provide a good understanding of the dynamic impingement process and provide insights on how surface wettability can affect the droplet spreading and rebounding process.

Keywords: Droplet impingement, two phase flow, hydrophobic surface, phase field method, dynamic contact angle

1. Introduction

The dynamic behavior of droplet impingement on a solid surface is important to many engineering applications, such as rain drops on automobile windshields, inkjet deposition and metal deposition in manufacturing processes, spray cooling of electronics, and spray coating for various applications. The droplet can spread, splash, and rebound after hitting a solid surface. The resulting phenomena and the final shape of the droplet on a surface depend on several parameters, including the properties of the droplet and the impacted surface, the droplet impact velocity, the droplet size, the angle of attack to the surface, the droplet physical properties, the surface wettability, and surrounding pressure [1]. One of the most challenging tasks of computations of droplet impingement is to incorporate the wetting effects into the numerical models [2,3].

The surface wettability is characterized by the contact angle formed between the liquid-vapor interface and the liquid-solid interface at the solid-liquid-vapor three phase contact line (or triple line) [4], as sketched in Fig. 1(a). When the contact line is stationary, the static (equilibrium) contact angle (SCA), θ_e, is ideally a unique property of the material system being considered. It can be measured experimentally and also determined by Young's equation.

$$\sigma cos\theta_e = \sigma_{sv} - \sigma_{sl} \quad (1)$$

where σ, σ_{sv}, and σ_{sl}, are respectively the surface tension of the liquid/vapor, solid/vapor, and solid/liquid surfaces.

However, in practice contact angle hysteresis arises, i.e. the equilibrium contact angle, θ_e, varies from the advancing contact angle, θ_a, to the receding contact angle, θ_r. The Young equilibrium contact angle is between these values as illustrated in Fig. 1(b). The contact angle hysteresis is measured by the difference between the advancing and receding contact angles, θ_a - θ_r.

When the contact line moves, the instantaneous contact angle is different from θ_e, and the angle is called dynamic contact angle, θ_d. As shown in Fig. 1 (b), the dynamic contact angle is a function of the contact line velocity, U_{cl}. Measuring the dynamic contact angle, θ_d, at the microscopic length scale close to the contact line is difficult in experiments, therefore, measurements were usually taken over a small but macroscopic length scale away from the wall

[5] for the apparent dynamic contact angle, θ^*_d. As shown schematically in Fig. 1(c), the dynamic contact angle, θ_d, is located in the inner region near the wall where the inertia is negligibly small while the apparent dynamic contact angle, θ^*_d. is in the outer region from the wall where inertia is not negligible. The inertia effects in the outer region will result in differences between θ_d and θ^*_d. Resolving the inner region in numerical simulations requires very fine grid near the contact line, therefore, the inner region is often neglected and contact angle models are applied for the apparent contact angle.

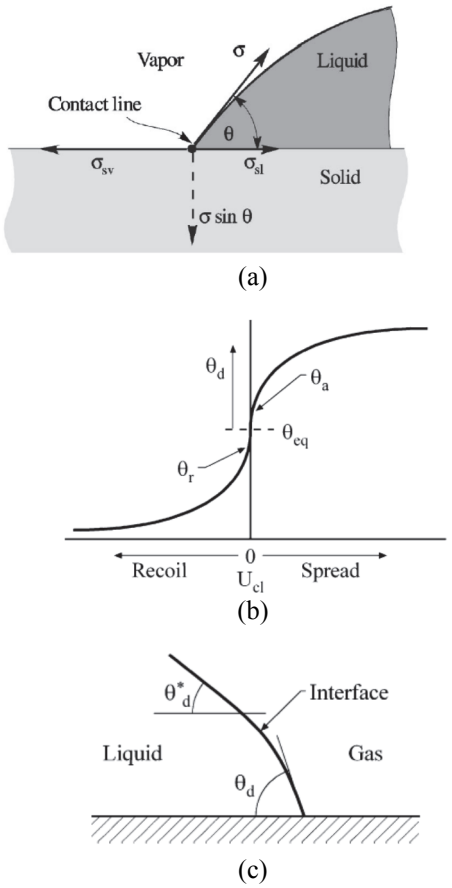

Fig. 1. Contact angles: (a) Schematic of equilibrium wetting line and contact angle (b) The static advancing, receding, and dynamic contact angles, θ_a, θ_r, and θ_d; (c) The dynamic contact angle, θ_d, and the apparent dynamic contact angle, θ^*_d [4, 5].

There are several empirical formulae relating the dynamic contact angle with the contact line velocity [6, 7]. In this study, the correlation given by Kistler [8] is employed to calculate the dynamic contact angle for each time step:

$$\theta_d = f_H\left[Ca + f_H^{-1}(\theta_e)\right] \tag{2}$$

Where f_H^{-1} is the inverse function of the Hoffman's function which is given in the following form:

$$f_H = \arccos\left\{1 - 2\tanh\left[5.16\left(\frac{x}{1+1.31x^{0.99}}\right)^{0.706}\right]\right\} \tag{3}$$

The capillary number, Ca, is defined as a function of the contact line velocity U_{cl}

$$Ca = \frac{\mu U_{cl}}{\sigma} \tag{4}$$

where μ is the dynamic viscosity of liquid.

It is important to incorporate the dynamic contact angle to account for its temporal evolution during the impinging process. However, it is not an easy process to implement the dynamic contact angle models in discretization based numerical schemes [2]. In many previous studies, a constant static contact angle (SCA) or advancing and receding contact angles are implemented as a wall boundary condition. The advancing-receding model is a quasi-dynamic contact angle (quasi-DCA) model, which can be represented by the following equation:

$$\theta_d = \begin{cases} \theta_a & \text{if } U_{cl} \geq 0 \\ \theta_r & \text{if } U_{cl} < 0 \end{cases} \tag{5}$$

This paper simulated the dynamic impinging process of a water droplet impacting on a dry wax substrate and studied the effects of contact angle on the droplet spreading and receding process. The numerical simulations were carried out using the Phase Field method in COMSOL. The droplet spreading and receding process was simulated with three contact angle models, including a constant static contact angle (SCA) model, a quasi-dynamic contact angle (quasi-DCA), and a dynamic contact angle (DCA) model using Kistler's law. The predicted spreading factor and apex height were compared with the experimental data of Sikalo and Ganic [9] and Sikalo et al. [10].

2. Use of COMSOL Multiphysics

The droplet impingement process is implemented with the Laminar Two-Phase Flow, Phase Field interface in COMSOL 4.3b. We have simulated a glycerin droplet impinging onto a hydrophobic surface and a hydrophilic surface using the Level Set method in COMSOL 4.3b [11]. The Phase Field method is found to be less sensitive to numerical parameters and thus numerically more stable than the Level Set method.

The 2D axisymmetric computational domain is shown in Fig. 2, where the water droplet is initially positioned at a certain distance above the substrate with an initial velocity. The droplet travels downward toward the substrate under the influence the gravity force and reaches the substrate at an impact velocity V_i.

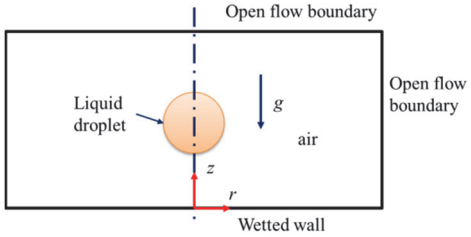

Figure 2. Schematic of computational domain

Open boundary conditions are used at the top and side to simulate an infinite domain. A wetted wall boundary condition is used for the substrate at the bottom. It sets the mass flow across the wall to be zero and specify the contact angle θ_w of fluid at the wall. This is prescribed by

$$\mathbf{n}\cdot\varepsilon^2\nabla\phi = \varepsilon^2\cos(\theta_w)|\nabla\phi| \quad (6)$$

$$\mathbf{n}\cdot\frac{\sigma\lambda}{\varepsilon^2}\nabla\psi = 0 \quad (7)$$

The paper studied a water droplet of 2.7 mm diameter impinging onto a solid wax surface with an impacting velocity of 1.17 m/s. The material properties of the water droplet and air are listed in Table 1. The Reynolds number, Weber number, and Ohnesorge number are calculated to be Re = 3100, We = 50, and Oh = 0.0023, respectively. According to Shiaffino and Sonin [12], the droplet impact behavior in this study is in the regime of hydrodynamic pressure-controlled flow.

The surface wettability of water on a wax surface was characterized by Sikalo and Ganic [9] and Sikalo et al. [10] as with a static advancing contact angle (θ_a = 105°) and a static receding contact angle (θ_r = 95°). The input for the contact angle at the wetted wall boundary is set as in Table 2 for the three different contact angle models.

Table 1. Properties of liquid and air

Parameter	Symbol	Value	unit
Density of water	ρ_l	998	kg/m^3
Dynamics viscosity of water	μ_l	0.001	Pa·s
Density of air	ρ_a	1.204	kg/m^3
Dynamics viscosity of air	μ_a	1.814×10^{-5}	Pa·s
Surface tension	σ	0.073	N/m

Table 2. Input for contact angle θ_w

Contact Angle Model	Value
SCA	95°, 100°, 105°
Quasi-DCA	Eq. (5)
DCA	Kistler's model

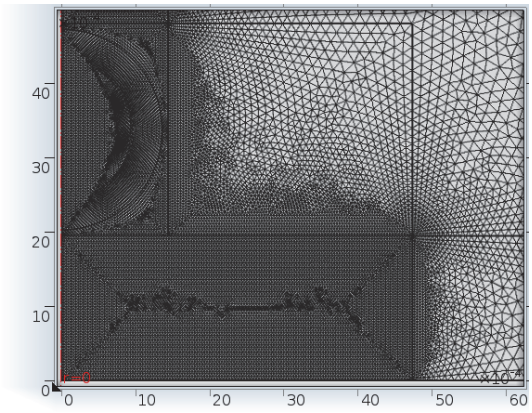

Figure 3. Mesh near the droplet impingement region

A non-uniform mesh of 449444 degrees of freedom (DOF) is used for the simulation. As shown in Fig. 3, the droplet impingment and droplet path region is covered with finer mesh and the mesh size gradually increases to the outer air domain. The smallest mesh size is 40 μm. The typical running time for each simulation is 11 hours on a workstation with Intel Xeon E5-2620 CPUs. Adaptive meshing

was tried with the simulation, but the results were not good. Therefore, a uniform mesh was set for the region where droplet travels.

4. Results

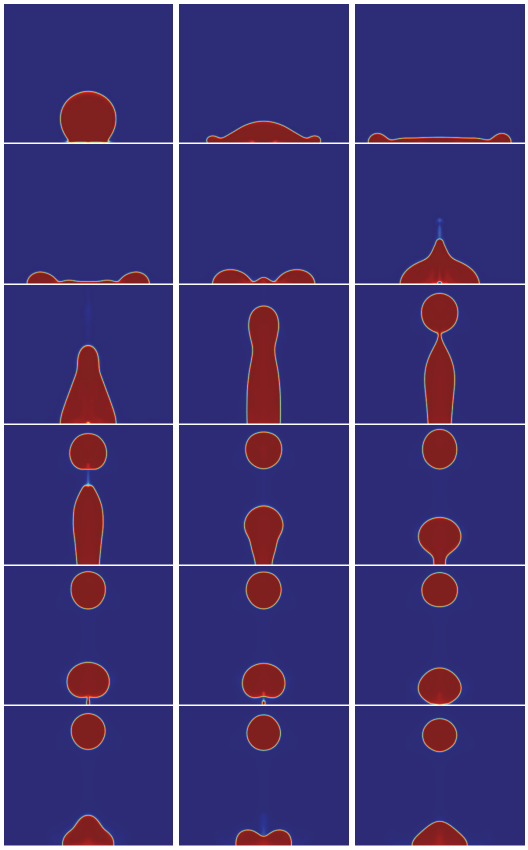

Figure 5. Droplet impingement process: t = 2.0, 3.5, 6.0, 9.0, 10.5, 12, 14, 19, 25.5, 26, 29, 31, 32, 32.25, 33.5, 36, 38, and 40 ms. The droplet reaches the surface at 1.8 ms. The simulation was conducted with the quasi-DCA model.

Figure 4 shows the simulation results of a sequence of droplet shape evolution at various time instants obtained with the quasi-DCA model. In this model the contact angle is set as the static advancing angle (θ_a) of 105° during the spreading process and the static receding angle of (θ_r) of 95° during the receding process. The droplet spreads under the impact pressure and reaches its maximum spreading radius around 6.0 ms. The flattened droplet then starts to recede under the capillary force. Two secondary droplets break up from the recoiling liquid column. The first break-up occurs at 25.6 ms. The remnant liquid column reverses its direction at the tip after the first break-up. However, it cannot reverse the flow direction at the substrate surface and a second break-up occurs at 32.25 ms. The second satellite droplet has a short rebound and then combines with the small volume of remnant liquid at the substrate.

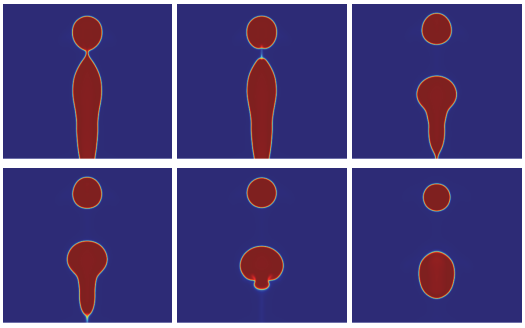

Figure 6. Droplet impingement process: t = 25.75, 26, 29.75, 30, 32, and 40 ms. The droplet reaches the surface at 1.8 ms. The simulation was conducted with the SCA model with a constant 100° contact angle.

The initial spreading process of other simulations are similar to those in Fig. 5. However, the droplet receding process is different and the resultant secondary droplet break-ups and droplet rebound depend on the contact angle setup. The simulation results of the droplet shape evolution obtained with a constant static contact angle (SCA) of 100° is shown in Fig. 6. The initial spreading phase is similar to that of Fig. 5, thus, only the later receding process is shown in Fig. 6. The higher contact angle at the receding stage leads to a secondary droplet break-up at 25.8 ms and the complete rebound of the remnant liquid at 29.9 ms. A complete rebound of the liquid column is obtained with a constant static contact angle of 100°.

Figs. 7 and 8 compare the dimensionless droplet wet diameter (spreading factor $\beta = d/D$) and droplet height (droplet height ratio h/D) obtained with the constant SCA models and the quasi-DCA model with the experimental data [9,10]. The early spreading process is driven by inertia, thus is independent of the contact angle input. The simulation results also agree well with the experimental data in the early spreading phase. Capillary force gradually plays a big role in the later spreading and receding phase, thus the simulation results depend on the contact

angle input. All the SCA and quasi-DCA models over predict the maximum spreading factor and a quicker recoil process. The simulation results obtained with the quasi-DCA model is better than the results obtained with the constant SCA models.

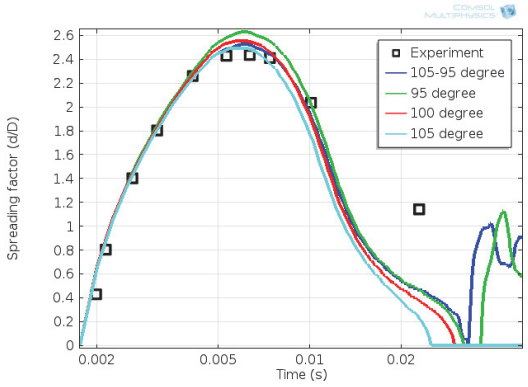

Figure 7. Spreading factor evolution of three SCA models (95º, 100º, and 105º) and the quasi-DCA model (105º - 95º).

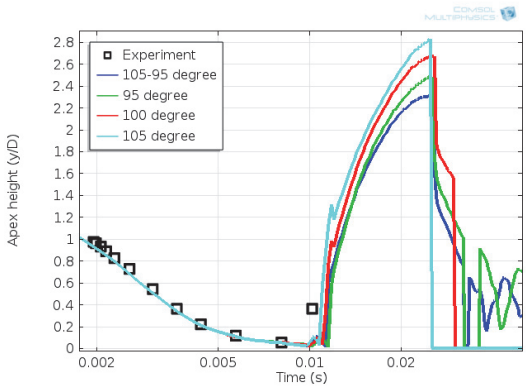

Figure 8. Apex height evolution of three SCA models (95º, 100º, and 105º) and the quasi-DCA model (105º - 95º).

Fig. 9 plots the evolution of the dynamic contact angle used in the quasi-DCA and DCA models. The dynamic contact angle varies with the contact line velocity, with values higher than the advancing static contact angle in the spreading phase and values lower than the receding contact angle in the receding phase. As it can be seen in Figs 10 and 11, the DCA model is able to predict more accurate spreading and receding process than a quasi-DCA model. However, the simulation results are still not close to the experimental results in the receding phase. Further work will be carried out on the choice of the dynamic contact angle models and the methods of calculating the contact line velocity in the future.

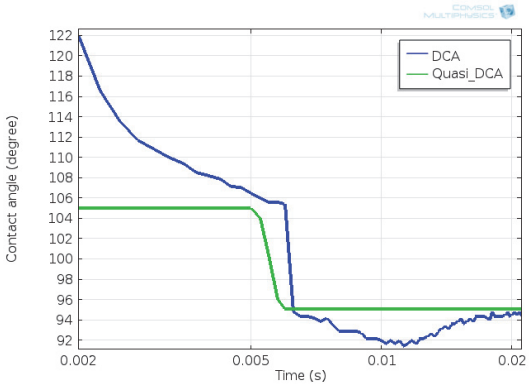

Figure 9. Dynamic contact angle evolution of the Quasi-DCA and DCA models.

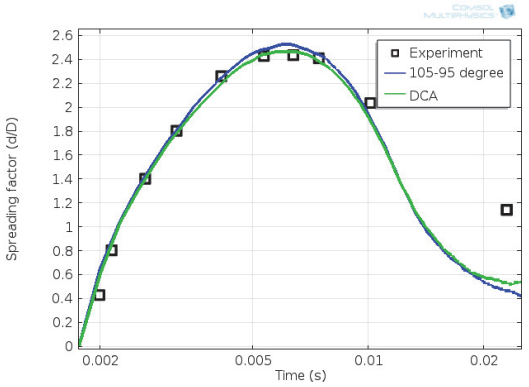

Figure 10. Spreading factor evolution of the quasi-DCA model (105º - 95º) and the DCA model.

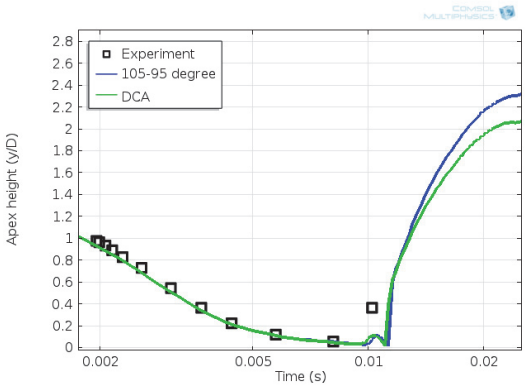

Figure 11. Apex height evolution of the quasi-DCA model (105º - 95º) and the DCA model.

5. Conclusions

This paper simulated the dynamic process of a water droplet impinging onto a wax substrate using the Phase Field method. The dynamic process of droplet evolutions was presented. The predicted spreading factor and apex height were validated against the experimental results. The effects of contact angles on the impingement process were also studied. The initial inertia driven spreading process is not affected by the input of the contact angle values, but the later spreading process and recoil process are significantly affected by the contact angle values. Higher contact angle during the advance stage lead to a smaller maximum spreading factor and a sooner rebound. The rebound liquid column is unstable with one or two secondary droplets form. It was found that a dynamic contact angle model is important for accurately modeling the droplet spreading and receding process. The instantaneous evolution of the dynamic contact angle cannot be represented by a constant static contact angle or the advancing-receding static contact angles. The simulation results can provide a good understanding of the dynamic impingement process and provide insights on how to control surface wettability to achieve a desired droplet spreading and rebounding process.

6. References

1. Amit Gupta and Ranganathan Kumar, Droplet impingement and breakup on a dry surface, *Computers and Fluids*, **39**, 1696-1703 (2010).

2. S. Ganesan, Simulations of impinging droplets with surfactant-dependent dynamic contact angle, *J. Comput. Phys.* **301** 178- 200 (2015).

3. Malgarinos, N. Nikolopoulos, M. Marengo, C. Antonini, M. Gavaises, VOF simulations of the contact angle dynamics during the drop spreading: standard models and a new wetting force model, *Advances in Colloid and Interface Science*, **212** 1-20 (2014).

4. S. Sikalo, H.-D. Wilhelm, I.V. Roisman, S. Jakirlic, C. Tropea, Dynamic contact angle of spreading droplets: experiments and simulations, *Phys. Fluids*, **17**, 062103 (2005).

5. Mukherjee S, Abraham J. Investigations of drop impact on dry walls with a lattice-Boltzmann model, *J Colloid Interface Sci.*, **312**, 341–54 (2007).

6. Roisman IV, Opfer L, Tropea C, Raessi M,Mostaghimi J, Chandra S., Drop impact onto a dry surface: Role of the dynamic contact angle, *Colloids Surf A Physicochem Eng Asp*, **322** 183–91 (2008).

7. T. Jiang, S. Oh, J.C. Slattery, Correlation for dynamic contact angle, *J. Colloid Interface Sci.*, **69** 74–77 (1979).

8. S.F. Kistler, Hydrodynamics of wetting, in: J.C. Berg (Ed.), Wettability, Marcel Dekker Inc., New York, 1993, pp. 311–429.

9. S. Sikalo and E.N. Ganic, Phenomena of droplet-surface interactions, *Experimental Thermal and Fluid Science*, **31**, 97-110 (2006).

10. S. Sikalo, M. Marengo, C. Tropea, and E.N. Ganic, Analysis of impact of droplets on horizontal surfaces, *Experimental Thermal and Fluid Science*, **25**, 503-510 (2002).

11. J. Hu, R., Jia, K.T. Wan, X. Xiong, Simulation of Droplet Impingement on a Solid Surface by the Level Set Method, 2014 COMSOL Conference in Boston, Boston, MA, Oct. 8-10, 2014.

12. S. Shiaffino and A.A. Sonin, Molten droplet deposition and solidification at low Weber numbers, *Phys. Fluids*, **9**, 3172-3187 (1997).